THE GEOLOGICAL SOCIETY OF AMERICA®

Glendonites track methane seepage in Mesozoic polar seas

Chloé Morales[1], Mikhail Rogov[2], Hubert Wierzbowski[3], Victoria Ershova[4], Guillaume Suan[5], Thierry Adatte[6], Karl B. Föllmi[6], Erik Tegelaar[7], Gert-Jan Reichart[1,8], Gert J. de Lange[1], Jack J. Middelburg[1], and Bas van de Schootbrugge[1]
[1]Department of Earth Sciences, Faculty of Geosciences, Utrecht University, Heidelberglaan 2, 3584 CS Utrecht, Netherlands
[2]Geological Institute, Russian Academy of Sciences (RAS), Pyzhevski lane 7, 119017 Moscow, Russia
[3]Polish Geological Institute, National Research Institute, Rakowiecka 4, 00-975 Warsaw, Poland
[4]Institute of Earth Sciences, St. Petersburg State University, Universitetskaya nab. 7/9, 199034 St. Petersburg, Russia
[5]Université Lyon 1, ENS-Lyon, CNRS, UMR 5276 LGL-TPE, F-69622 Villeurbanne, France
[6]Institute of Earth Sciences, University of Lausanne, Géopolis, 1015 Lausanne, Switzerland
[7]Shell International Ltd., Kessler Park 1, 2288 GS Rijswijk, Netherlands
[8]Royal Netherlands Institute for Sea Research (NIOZ), Ocean Sciences Department, PO Box 59, 1790 AB Den Burg, Texel, Netherlands

ABSTRACT

During the Phanerozoic, Earth has experienced a number of transient global warming events associated with major carbon cycle perturbations. Paradoxically, many of these extreme greenhouse episodes are preceded or followed by cold climate, perhaps even glacial conditions, as inferred from the occurrence of glendonites in high latitudes. Glendonites are pseudomorphs of ikaite ($CaCO_3 \cdot 6H_2O$), a hydrated carbonate mineral increasingly stable at low temperatures. Here, we show that methane seepage and oxidation provide an overriding control on Mesozoic glendonite formation (i.e., ikaite fossilization). Geochemical and petrological analyses of 33 Early Jurassic to Early Cretaceous glendonites from five sections in Siberia (Russia) reveal that most of their infilling carbonate phases are reminiscent of methane-derived authigenic carbonates. Bulk glendonites and surrounding sediments exhibit exceptionally high and low carbon isotope values (+20‰ to −45‰ VPDB [Vienna Peedee belemnite]), typical for carbon sources linked to methane generation and oxidation. Gas inclusion data confirm the presence of methane and longer-chain hydrocarbon gases, suggesting a thermogenic source for the methane. Glendonite-bearing layers can be traced for hundreds of kilometers, suggesting widespread trapping of methane in the sub-seafloor during the Jurassic. As such, glendonites constitute an unexplored archive for detecting past episodes of methane release and oxidation in polar settings.

INTRODUCTION

Methane is a potent greenhouse gas, with multiple natural sources including marine cold seeps and gas hydrates. Authigenic carbonates associated with the anaerobic oxidation of methane (AOM) can be used to document the distribution in time and space of oceanic methane seepage (Peckmann et al., 1999) and its links to carbon cycle perturbations and climate change (Sun and Turchyn, 2014). One such authigenic carbonate mineral, ikaite ($CaCO_3 \cdot 6H_2O$), which can become fossilized as glendonite, remains poorly understood. The stability of ikaite is favored by low temperatures, and the mineral rapidly decomposes above 7 °C (Pauly, 1963). Three main types of ikaite are distinguished: (1) tufa and travertines in springs and alkaline lakes (Pauly, 1963; Shearman et al., 1989), (2) single microscopic crystals in Arctic and Antarctic ice (Dieckmann et al., 2010), and (3) macroscopic single euhedral to stellate crystal clusters found in marine sediments. The latter ikaite type is thought to form during early diagenesis. It has a wide range of $\delta^{13}C_{carb}$ (carb—carbonate) values (from −57‰ to +4‰; Kodina et al., 2003, Lu et al., 2012), which has been attributed to the mixing of carbon generated during organic matter degradation, methanogenesis, and AOM (Kodina et al., 2003; Lu et al., 2012). The term "glendonite" pertains to pseudomorphs after this type of ikaite (David and Taylor, 1905). The transformation of ikaite to glendonite is thought to result from the slow decrease in the concentration of Ca^{2+} and CO_3^{2-} and high phosphate levels as ikaite grows (Bischoff et al., 1993), or to a change of carbon source and pore-water chemistry from sulfate reduction of organic-rich sediments to AOM-driven processes linked to burial and vent activity in the Sea of Okhotsk (Greinert and Derkachev, 2004).

Although ikaite formation has been linked to *in situ* methane generation and oxidation in previous work (Kodina et al., 2003; Lu et al., 2012), glendonites have thus far mostly been used as a proxy record for cold temperatures, due to the peculiar thermodynamic parameters that control ikaite formation. Emphasis has been put on the reconstruction of seawater temperature from bulk glendonite $\delta^{18}O_{carb}$ values, but unexpectedly low $\delta^{18}O_{carb}$ values have proved ambiguous (Price and Nunn, 2010). Besides, and similarly to ikaite, glendonites show $\delta^{13}C$ values ranging from −45‰ to 0‰ (Selleck et al., 2007; Teichert and Luppold, 2013), suggesting a connection between certain glendonite-bearing sites and methane seepage (Greinert and Derkachev, 2004; Teichert and Luppold, 2013). Based on petrological and geochemical analyses on glendonites and host sediments, as well as on the molecular and isotopic composition of gas inclusions trapped in glendonites, we demonstrate that the ikaite-to-glendonite transformation was an early diagenetic process linked to AOM. Glendonites may thus be used to document past events of methane release and oxidation in cold environments.

GEOLOGICAL SETTING AND METHODS

A total of 33 glendonites were sampled from five sections in Siberia (Russia), composed of marine sandstone, siltstone, and mudstone, spanning the late Pliensbachian (Anabar Bay; Suan et al., 2011), the late Bajocian (Cape Kystatym and Cape Khorongkho), the late Bajocian–early Bathonian (Chekurovka), and the early Bathonian and late Berriasian (Chucha) (Figs. 1A and 1B). The sedimentary successions were deposited in shallow to deep continental shelf settings (corresponding to shoreface to offshore environments) near the North Pole (Fig. 1C; see the GSA Data Repository[1]). The sampled sections are stratigraphically constrained by the occurrence of age-diagnostic ammonites, brachiopods, and bivalves, as well as accessory microfossils and chemostratigraphy in the Anabar Bay section (see the Data Repository). Except for some specimens found in a conglomerate bed, none of the glendonites were transported (shown by the preservation of their angular shape). All glendonites and enclosing nodules and sediments were subjected to petrographical (optical and ultraviolet-light microscope), bulk stable isotope (inorganic carbon and

[1]GSA Data Repository item 2017159, coordinates of the sections, details on stratigraphy, methods and geochemical results (Rock-Eval and CSIA), and tables of raw geochemical data, is available online at http://www.geosociety.org/datarepository/2017/ or on request from editing@geosociety.org.

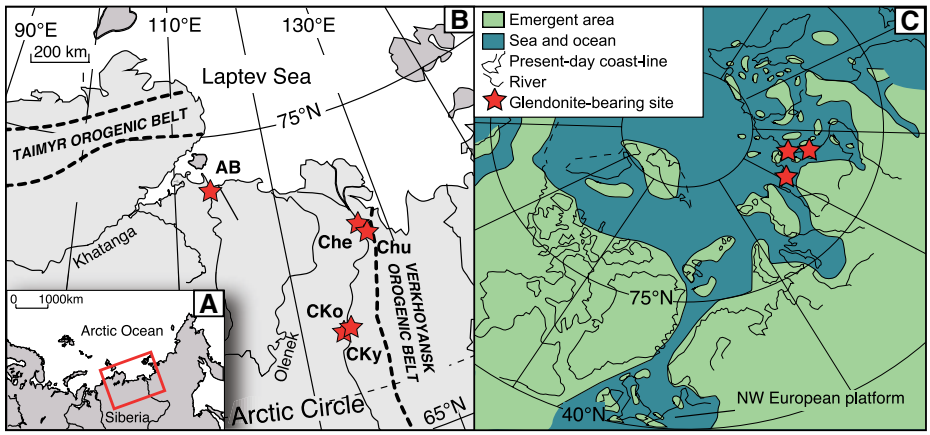

Figure 1. A,B: Location of North Siberian Basin (Russia), with red stars denoting location of sampled sections along Lena River (CKy—Cape Kystatym; CKo—Cape Khorongkho; Chu—Chucha; Che—Chekurovka) and along Laptev Sea (AB—Anabar Bay), modified after Suan et al. (2011). C: Paleogeographic map of Early Jurassic (late Pliensbachian) showing past locations of glendonite formation (after Meledina et al., 2005).

oxygen), and Rock-Eval (Espitalié et al., 1985) analyses. Gas inclusions of glendonites were examined by compound-specific isotope analyses (CSIA) on five selected specimens.

PETROLOGICAL CHARACTERISTICS

Thin-section analyses of the investigated glendonites reveal a number of genetic phases of carbonate growth alternating with phases of dissolution (Fig. 2). The following genetic phases are recurrent, independent of location and age:

(1) Whitish calcite crystals organized into "rosettes", containing organic matter impurities and which are overgrown by replacive calcite cements. Rosettes likely result from the direct recrystallization of ikaite into calcite (Teichert and Luppold, 2013).

(2) Fibrous to botryoidal carbonates in different shades of yellowish amber, in some cases also characterizing nodules surrounding glendonites.

(3) Anhedral irregular to clotted amber-colored calcites that have recrystallized part (or most) of the glendonite.

In a conglomerate bed at Cape Kystatym (Bajocian-Bathonian; Fig. 2F), reworked glendonites bear genetic phases 1 and 2, which are equally observed in Quaternary ikaites from the Nankaï Trough (Stein and Smith, 1986). Hence, these cements precipitated during very early diagenesis. Similar cementation patterns have been observed in glendonites from distant regions and different age (Greinert and Derkachev, 2004; Huggett et al., 2005; Teichert and Luppold, 2013), indicating that they represent widespread features of ikaite fossilization.

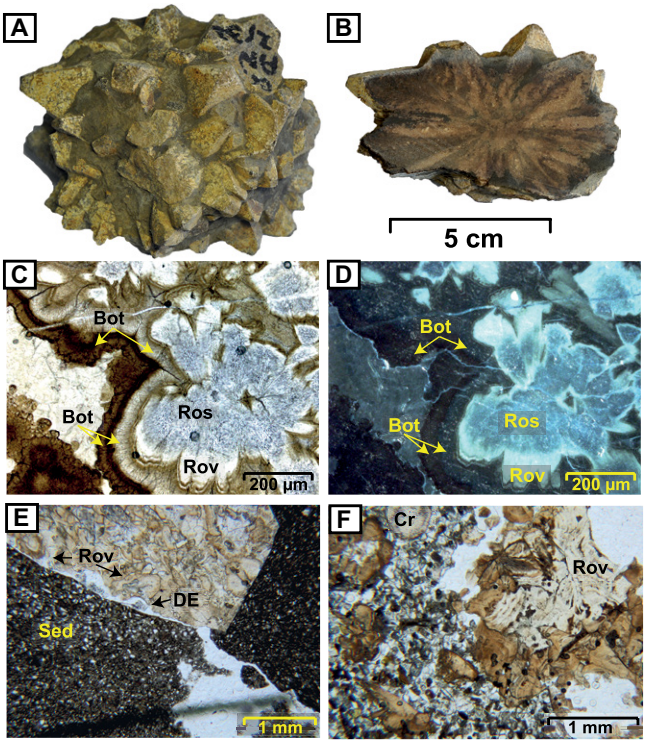

Figure 2. Macroscopic and microscopic views of glendonite specimens from Siberia (Russia). A,B: Medium-size stellate-shape glendonite; upper Pliensbachian, profile and transverse views, respectively. C,D: Succession of carbonate cements observed in glendonites (Ros—rosette oriented crystals; Rov—rosette calcite overgrowths; Bot—botryoids); upper Bajocian, transmitted and ultraviolet light (UV), respectively. Rosettes contain black UV-fluorescent impurities resulting from organic particles. Some botryoidal carbonates have highly fluorescent rim that may be due to microbial film. E: Fluid exhaust microstructure associated with dissolution event (DE) disbanding rosette overgrowths (Rov) of glendonite and reworking nonconsolidated host sediment (Sed); upper Bajocian. F: Conglomerate of reworked and broken glendonites containing rosette overgrowths (Rov) in sandy matrix with crinoid fragments (Cr), and highlighting early fossilization of ikaite; upper Bajocian.

CARBON AND OXYGEN ISOTOPE DATA

The occurrence of fibrous/botryoidal carbonates in high latitudes, in association with clotted and anhedral carbonates (genetic phase 3) and repeated dissolution events, is reminiscent of mineralogical features described from hydrocarbon seep carbonates (Savard et al., 1996). A link to hydrocarbon oxidation is also apparent from stable isotope analyses. Glendonite samples show bulk $\delta^{13}C_{carb}$ and $\delta^{18}O_{carb}$ values ranging from –44.5‰ to 0‰ VPDB (Vienna Peedee belemnite) and from –14.7‰ to –0.8‰ VPDB, respectively, displaying a generally strong inverse correlation (Fig. 3). Carbonate nodules surrounding glendonites have less-variable $\delta^{13}C_{carb}$ and $\delta^{18}O_{carb}$ values, ranging between –30.4‰ and –16.4‰ VPDB and –4.0‰ to –2.7‰ VPDB, respectively. Diagenetic carbonates of bulk sediment enclosing glendonites exhibit low to exceptionally high $\delta^{13}C_{carb}$ values ranging from –29.5‰ to +21.3‰ VPDB, and $\delta^{18}O_{carb}$ values between –2.6‰ and –20.6‰ VPDB. A late diagenetic overprint of bulk sediment carbon and oxygen isotope values cannot be completely ruled out (Jacobsen and Kaufman, 1999). Cracking temperatures of organic material (T_{max}) show a wide range of values (between 412 and 482 °C) corresponding to immature and mature material. However, this large uncertainty can be ascribed to very low values of S2 peaks linked to an intense oxidation of the organic material, and to low total organic contents (TOC) (Behar et al., 2001). Jurassic sediments on the Siberian craton were probably never deeply buried (Drachev et al., 2010). The preservation of aragonitic bivalves and T_{max} data of Suan et al. (2011) also suggest that sediments only reached the uppermost part of the oil window. In our samples, sparry (blocky) calcite related to burial cementation represents only a minor carbonate phase, and no correlation has been observed between its relative occurrence and changes in $\delta^{18}O$ and $\delta^{13}C$ values.

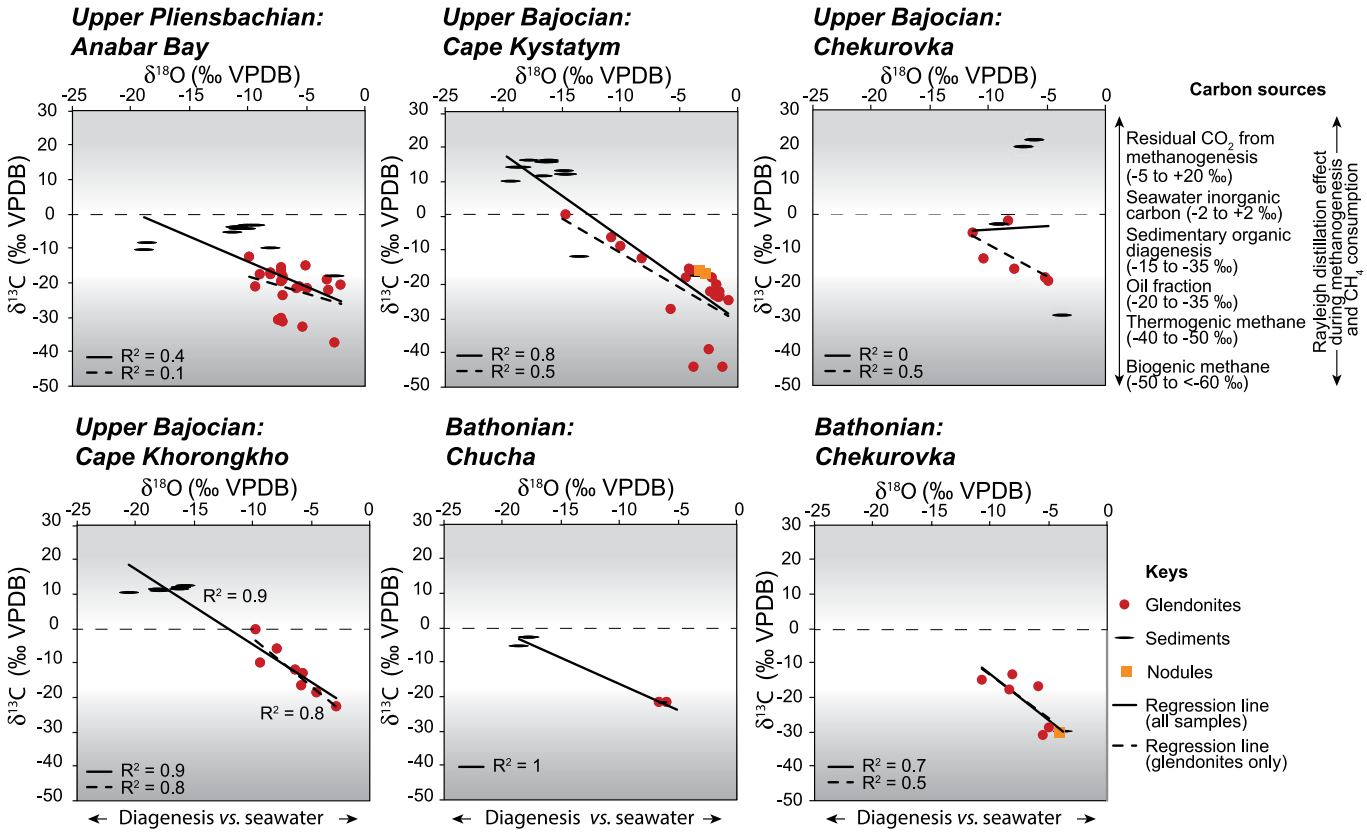

Figure 3. Carbon and oxygen stable isotope distribution of carbonates belonging to bulk glendonites from Siberia (Russia; see Fig. 1 for sample locations), surrounding nodules, and enclosing sediment. Methane oxidation is a central process contributing to carbonate carbon sources. VPDB—Vienna Peedee belemnite.

The isotopic data from bulk glendonite samples can be separated into two groups. The first has normal marine $\delta^{18}O_{carb}$ values (up to –0.8‰ VPDB) that are accompanied by extremely low $\delta^{13}C_{carb}$ values (–25‰ to –45‰ VPDB), implicating methane as a carbon source. The less-negative $\delta^{13}C_{carb}$ values obtained for some glendonites (~–25‰ VPDB) could be related to the mixing of various carbon sources and geochemical processes, including aerobic oxidation of organic matter, sulfate reduction, and/or fermentation (Whiticar, 1999), or to a changing proportion of biogenic versus thermogenic methane. The second group is strongly ^{13}C enriched, which is explained by a residual CO_2 source from microbial methanogenesis. The ^{18}O-depleted values indicate the late diagenetic circulation of fluids (Jacobsen and Kaufman, 1999).

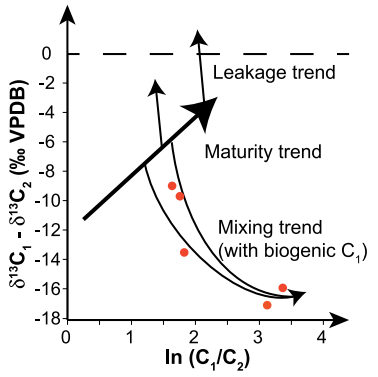

Figure 4. Model of gas genetic fractionation based on analyses of relative hydrocarbon composition of glendonites and their specific stable carbon isotope content. Leakage and mixing can influence the molecular and isotopic composition of hydrocarbon gases at various stages of gas maturation (narrow arrows). The $\delta^{13}C_1$-$\delta^{13}C_2$ versus ln(C1/C2) diagram (Prinzhofer and Huc, 1995) confirms occurrence of mixed thermogenic and biogenic methane within glendonite samples. VPDB—Vienna Peedee belemnite.

IMPLICATION OF GAS INCLUSIONS FOR FORMATION OF GLENDONITES

Compound-specific isotope analyses performed on gas inclusions of bulk glendonites (Fig. 4) document the average gas composition during the ikaite-to-glendonite transformation. In addition to methane (C_1), significant concentrations of higher-molecular-weight hydrocarbon gases (C_{2+}), including ethane (C_2), propane (C_3), butane (C_4), and pentane (C_5), were detected. The investigated glendonites samples have $\delta^{13}C_{carb}$ values between –13‰ and –28‰ VPDB, showing the limitations of bulk $\delta^{13}C_{carb}$ values as proxies for the role of methane in authigenic carbonate precipitation. Biogenic degradation of organic matter produces strongly ^{12}C-enriched methane (up to –110‰ VPDB), whereas thermogenic cracking leads to the formation of various hydrocarbon gases (C_1 to C_5) with a $\delta^{13}C$ signature closer to that of the parent organic matter (–30‰ to –50‰ VPDB; Schoell, 1980). A gas interpretation plot (Prinzhofer and Huc, 1995) shows that a mixture of thermogenic and biogenic hydrocarbon gas was likely involved in ikaite/glendonite formation at the investigated locations (Fig. 4). The proportion of biogenic and thermogenic methane is difficult to evaluate due to additional CO_2-reduction and Rayleigh-distillation processes (Whiticar, 1999). However, the high concentration of C_{2+} gas (varying between 5%–28% of total hydrocarbons) and C_1 / (C_2 + C_3) ratios between 3 and 24 (Martin et al., 1997) indicate a major contribution of thermogenic gas in the inclusions (Schoell, 1980). Especially propane, which is known to be rapidly biodegraded both anaerobically and aerobically (Kinnaman et al., 2007; Quistad and Valentine, 2011), shows no significant carbon isotope fractionation. This confirms the very rapid transformation of ikaite to glendonite and argues against a slow late diagenetic incorporation of hydrocarbons during the recrystallization of carbonates.

A local (i.e., *in situ*) methane source equally appears questionable, as glendonites are associated with clay, silt, and sandstone, which have a very low TOC (0–0.8 wt%, see the Data Repository). Conversely, glendonites

are not observed in certain nearby sections where TOC values are higher (Suan et al., 2011). Methane was likely sourced from a deeper reservoir with thermogenic methane diffusing upwards, perhaps linked to the activity of the Verkhoyansk and Taimyr fault zones (Fig. 1). Typical seep structures and fauna are not observed, suggesting that methane did not reach the sediment-water interface and that fluxes were diffusive (Teichert and Luppold, 2013).

CONCLUSIONS

Our new multi-proxy data set clearly demonstrates that Siberian glendonites record the occurrence of methane seepage during the Jurassic and the Early Cretaceous. Their occurrence is decoupled from local TOC content, pointing to a deeper hydrocarbon source. The complex sequence of ikaite-calcite precipitation leading to glendonite formation, as well as the large range of $\delta^{18}O_{carb}$ values found here, prevent the use of bulk glendonite $\delta^{18}O_{carb}$ values to monitor past seawater temperatures. Instead, the relationship between glendonite formation and methane oxidation is of interest with regards to past intervals of global carbon cycle perturbations. The Toarcian oceanic anoxic event (OAE), the Valanginian Weissert event, the Aptian-Albian OAEs, and to some extent the Paleocene-Eocene Thermal Maximum (Kaplan, 1978; Kemper, 1987; Price, 1999; Spielhagen and Tripati, 2009) were all accompanied by widespread glendonite formation.

ACKNOWLEDGMENTS

We thank three anonymous reviewers and Jörn Peckman for constructive feedback, as well as Otto H. Stiekema and Arnold E. van Dijk for their technical assistance. The Swiss National Science Foundation (grant P2LAP2-155097 to Morales), The Netherlands Organisation for Scientific Research (project n° NWO ALWOP.145 to van de Schootbrugge), Utrecht University, the Russian State program (grant 0135-2014-0064, Geological Institute, RAS), Program II.3 (RAS), the Russian Foundation for Basic Research (grant 15-05-03149 to Rogov), and Shell International (Netherlands) are acknowledged for their financial support and access to laboratory facilities. This research contributes to the Netherlands Earth System Sciences Center.

REFERENCES CITED

Behar, F., Beaumont, V., and Penteado, H.L.D.B., 2001, Rock-Eval 6 technology: Performances and developments: Oil & Gas Science and Technology, v. 56, p. 111–134, doi:10.2516/ogst:2001013.

Bischoff, J.L., Fitzpatrick, J.A., and Rosenbauer, R.J., 1993, The solubility and stabilization of ikaite ($CaCO_3 \cdot 6H_2O$) from 0° to 25°C: Environmental and paleoclimatic implications for thinolite tufa: The Journal of Geology, v. 101, p. 21–33, doi:10.1086/648194.

David, T.W., and Taylor, T.G., 1905, Occurrence of the pseudomorph glendonite in New South Wales, Sydney: Records of the Geological Survey of New South Wales, v. 8, p. 161–179.

Dieckmann, G., Nehrke, G., Uhlig, C., Göttlicher, J., Gerland, S., Granskog, M.A., and Thomas, D.N., 2010, Ikaite ($CaCO_3 \cdot 6H_2O$) discovered in Arctic sea ice: The Cryosphere, v. 4, p. 227–230, doi:10.5194/tc-4-227-2010.

Drachev, S.S., Malyshev, N.A., and Nikishin, A.M., 2010, Tectonic history and petroleum geology of the Russian Arctic Shelves: An overview, *in* Vining, B.A., and Pickering, S.C., eds., Petroleum Geology: From Mature Basins to New Frontiers—Proceedings of the 7th Petroleum Geology Conference: Geological Society of London Petroleum Geology Conference Series 7, p. 591–619, doi:10.1144/0070591.

Espitalié, J., Deroo, G., and Marquis, F., 1985, La pyrolyse Rock-Eval et ses applications: Revue de l'Institut Français du Pétrole, v. 40, p. 563–579.

Greinert, J., and Derkachev, A., 2004, Glendonites and methane-derived Mg-calcites in the Sea of Okhotsk, Eastern Siberia: Implications of a venting-related ikaite/glendonite formation: Marine Geology, v. 204, p. 129–144, doi:10.1016/S0025-3227(03)00354-2.

Huggett, J.M., Schultz, B.P., Shearman, D.J., and Smith, A.J., 2005, The petrology of ikaite pseudomorphs and their diagenesis: Proceedings of the Geologists' Association, v. 116, p. 207–220, doi:10.1016/S0016-7878(05)80042-2.

Jacobsen, S.B., and Kaufman, A.J., 1999, The Sr, C and O isotopic evolution of Neoproterozoic seawater: Chemical Geology, v. 161, p. 37–57, doi:10.1016/S0009-2541(99)00080-7.

Kaplan, M.E., 1978, Calcite pseudomorphs in Jurassic and Lower Cretaceous deposits of the northern area of eastern Siberia: Geologiya i Geofizika (Russian Geology and Geophysics), v. 19, p. 62–70.

Kemper, E., 1987, Das Klima der Kreide-Zeit, Hannover, Bundesanstalt für Geowissenschaften und Rohstoffe und Geologische Landesämter in der Bundesrepublik Deutschland, Geologisches Jahrbuch Reihe A: Allgemeine und regionale Geologie Bundesrepublik Deutschland und Nachbargebiete, Tektonik, Stratigraphie, Paläontologie: Stuttgart, Germany, Schweizerbart, 96 p. (in German).

Kinnaman, F.S., Valentine, D.L., and Tyler, S.C., 2007, Carbon and hydrogen isotope fractionation associated with the aerobic microbial oxidation of methane, ethane, propane and butane: Geochimica et Cosmochimica Acta, v. 71, p. 271–283, doi:10.1016/j.gca.2006.09.007.

Kodina, L.A., Tokarev, V.G., Vlasova, L.N., and Korobeinik, G.S., 2003, Contribution of biogenic methane to ikaite formation in the Kara Sea: Evidence from the stable carbon isotope geochemistry, *in* Stein, R., et al., eds., Siberian River Run-Off in the Kara Sea: Characterisation, Quantification, Variability and Environmental Significance: Amsterdam, Elsevier, Proceedings in Marine Sciences, v. 6, p. 349–374.

Lu, Z., Rickaby, R.E.M., Kennedy, H., Kennedy, P., Pancost, R.D., Shaw, S., Lennie, A., Wellner, J., and Anderson, J.B., 2012, An ikaite record of late Holocene climate at the Antarctic Peninsula: Earth and Planetary Science Letters, v. 325–326, p. 108–115, doi:10.1016/j.epsl.2012.01.036.

Martin, J.B., Orange, D.L., Lorenson, T.D., and Kvenvolden, K.A., 1997, Chemical and isotopic evidence of gas-influenced flow at a transform plate boundary: Monterey Bay, California: Journal of Geophysical Research, v. 102, p. 24,903–24,915, doi:10.1029/97JB02154.

Meledina, S.V., Shurygin, B.N., and Dzyuba, O.S., 2005, Stages in development of mollusks, paleobiogeography of Boreal seas in the Early–Middle Jurassic and zonal scales of Siberia: Geologiya i Geofizika (Russian Geology and Geophysics), v. 46, p. 239–254.

Pauly, H., 1963, "Ikaite," a new mineral from Greenland: Arctic, v. 16, p. 263–264, doi:10.14430/arctic3545.

Peckmann, J., Thiel, V., Michaelis, W., Clari, P., Gaillard, C., Martire, L., and Reitner, J., 1999, Cold seep deposits of Beauvoisin (Oxfordian; southeastern France) and Marmorito (Miocene; northern Italy): Microbially induced authigenic carbonates: International Journal of Earth Sciences, v. 88, p. 60–75, doi:10.1007/s005310050246.

Price, G.D., 1999, The evidence and implications of polar ice during the Mesozoic: Earth-Science Reviews, v. 48, p. 183–210, doi:10.1016/S0012-8252(99)00048-3.

Price, G.D., and Nunn, E.V., 2010, Valanginian isotope variation in glendonites and belemnites from Arctic Svalbard: Transient glacial temperatures during the Cretaceous greenhouse: Geology, v. 38, p. 251–254, doi:10.1130/G30593.1.

Prinzhofer, A.A., and Huc, A.Y., 1995, Genetic and post-genetic molecular and isotopic fractionations in natural gases: Chemical Geology, v. 126, p. 281–290, doi:10.1016/0009-2541(95)00123-9.

Quistad, S.D., and Valentine, D.L., 2011, Anaerobic propane oxidation in marine hydrocarbon seep sediments: Geochimica et Cosmochimica Acta, v. 75, p. 2159–2169, doi:10.1016/j.gca.2011.02.001.

Savard, M.M., Beauchamp, B., and Veizer, J., 1996, Significance of aragonite cements around Cretaceous marine methane seeps: Journal of Sedimentary Research, v. 66, p. 430–438, doi:10.1306/D4268365-2B26-11D7-8648000102C1865D.

Schoell, M., 1980, The hydrogen and carbon isotopic composition of methane from natural gases of various origins: Geochimica et Cosmochimica Acta, v. 44, p. 649–661, doi:10.1016/0016-7037(80)90155-6.

Selleck, B.W., Carr, P.F., and Jones, B.G., 2007, A review and synthesis of glendonites (pseudomorphs after ikaite) with new data: Assessing applicability as recorders of ancient coldwater conditions: Journal of Sedimentary Research, v. 77, p. 980–991, doi:10.2110/jsr.2007.087.

Shearman, D.J., McGugan, A., Stein, C., and Smith, A.J., 1989, Ikaite, $CaCO_3 \cdot 6H_2O$, precursor of the thinolites in the Quaternary tufas and tufa mounds of the Lahontan and Mono Lake Basins, western United States: Geological Society of America Bulletin, v. 101, p. 913–917, doi:10.1130/0016-7606(1989)101<0913:ICOPOT>2.3.CO;2.

Spielhagen, R.F., and Tripati, A., 2009, Evidence from Svalbard for near-freezing temperatures and climate oscillations in the Arctic during the Paleocene and Eocene: Palaeogeography, Palaeoclimatology, Palaeoecology, v. 278, p. 48–56, doi:10.1016/j.palaeo.2009.04.012.

Stein, C.L., and Smith, A.J., 1986, Authigenic carbonate nodules in the Nankai Trough, Site 583, *in* Kagami, H., Karig, D.E., Coulbourn, W.T., et al., Initial Reports of the Deep Sea Drilling Project, Volume 87: Washington, D.C., U.S. Government Printing Office, p. 659–668.

Suan, G., et al., 2011, Polar record of Early Jurassic massive carbon injection: Earth and Planetary Science Letters, v. 312, p. 102–113, doi:10.1016/j.epsl.2011.09.050.

Sun, X., and Turchyn, A.V., 2014, Significant contribution of authigenic carbonate to marine carbon burial: Nature Geoscience, v. 7, p. 201–204, doi:10.1038/ngeo2070.

Teichert, B.M.A., and Luppold, F.W., 2013, Glendonites from an Early Jurassic methane seep: Climate or methane indicators?: Palaeogeography, Palaeoclimatology, Palaeoecology, v. 390, p. 81–93, doi:10.1016/j.palaeo.2013.03.001.

Whiticar, M.J., 1999, Carbon and hydrogen isotope systematics of bacterial formation and oxidation of methane: Chemical Geology, v. 161, p. 291–314, doi:10.1016/S0009-2541(99)00092-3.

Manuscript received 9 November 2016
Revised manuscript received 2 February 2017
Manuscript accepted 2 February 2017

Printed in USA

Supplemental Information 1: Calculated palaeolatitudes for all studied sections, derived through http://palaeolatitude.org (van Hinsbergen et al., 2015; paleomagnetic reference frame after Torsvik et al., 2012)

Locality	Age	Coordinates (current)	Palaeolatitude
Anabar Bay	Late Pliensbachian	73.386854936347 N; 113.322601318359 E	82.7 N
Cape Kystatym	Late Bajocian	67.363129011005 N; 123.180084228515 E	84.52 N
Cape Khorongkho	Late Bajocian	67.273103809385 N; 123.120346069335 E	84.49 N
Chekurovka	Late Bajocian - Early Bathonian	70.997741629904 N; 127.55092620849 E	84.95 N
Cape Chucha	Early Bathonian	70.788717462945 N; 127.591781616210 E	85.07 N
Cape Chucha	Late Berriasian	70.788717462945 N; 127.591781616210 E	71.64 N

References:

van Hinsbergen, D. J. J., L. V. de Groot, S. J. van Schaik, W. Spakman, P. K. Bijl, A. Sluijs, C. G. Langereis and H. Brinkhuis (2015). "A paleolatitude calculator for paleoclimate studies." PloS one **10**(6): e0126946.

Torsvik, T. H., R. Van der Voo, U. Preeden, C. Mac Niocaill, B. Steinberger, P. V. Doubrovine, D. J. J. van Hinsbergen, M. Domeier, C. Gaina and E. Tohver (2012). "Phanerozoic polar wander, palaeogeography and dynamics." Earth-Science Reviews **114**(3): 325-368.

Supplemental Information 2: Stratigraphic logs and position of the glendonite-bearing layers

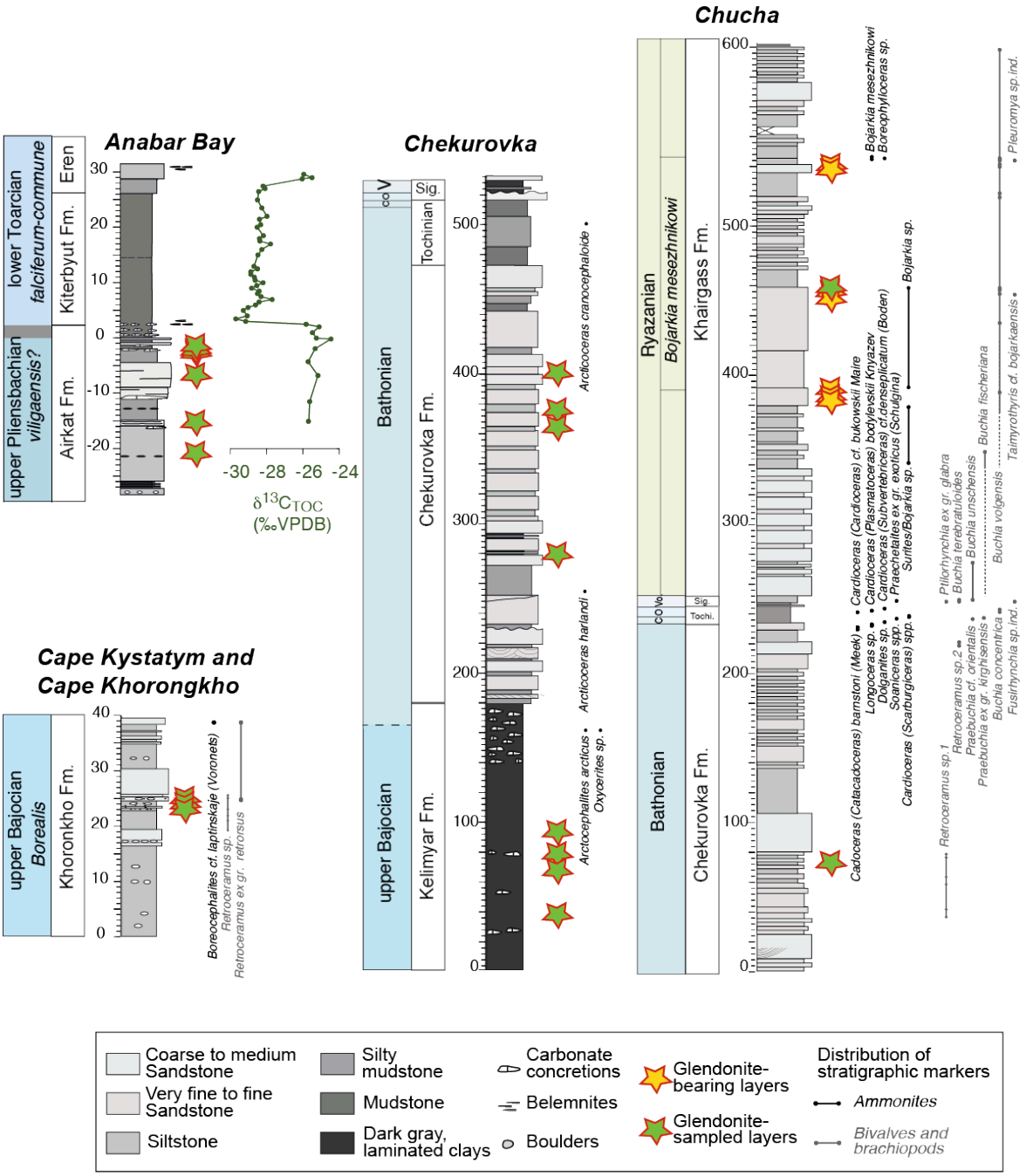

Supplemental Information 3: Stratigraphy of glendonite-bearing layers, and precisions on correlation between the Boreal and International Time Scales

The Anabar Bay[1], Cape Kystatym[2], Cape Khorongkho[2], Chekurovka[3] and Chucha[2] sections expose marine sandstone, siltstone and mudstone from the Lower and Middle Jurassic, and from the Early Cretaceous. The sedimentary successions were deposited in shallow to deep continental shelf settings (corresponding to shoreface to offshore environments), near the North Pole. Macrofossils include abundant wood debris and bivalves, as well as a few belemnites rostra, gastropods, brachiopods, and ammonites. The latter assign glendonite-bearing layers to a relatively accurate stratigraphic framework.

1. Upper Pliensbachian: Anabar Bay

The Lower Jurassic section of Anabar Bay is characterized by a set of biostratigraphic and geochemical tools[4,1]. Ammonites are very uncommon and poorly preserved in this succession. Although the index species of the *Amaltheus viligaensis* ammonite zone have not been recorded here, an upper Pliensbachian *Amaltheus* sp. age assignation is nevertheless attributed by correlation with dinocyst and bivalve stratigraphies, which nearly corresponds to the *Spinatum* zone of the Geological Time Scale.

2. Upper Bajocian: Cape Kystatym, Cape Khorongho and Chekurovka

In the north of Siberia, the upper Bajocian is marked by the first appearance datum of the ammonite family *Cardioceratidae*. The lower boundary of the ammonite zone *Cranocephalites borealis* is considered as nearly equivalent of the lower-upper Bajocian boundary because: (1) the ammonite *Sphaeroceras (Defonticeras)*, which is considered as ancestor of *Cranocephalites*, is known from the uppermost zone of the Lower Bajocian[5]; (2) Strontium isotope values derived from deposits belonging to the *Cranocephalites borealis* ammonite zone in East Greenland, (basal part of the Pelion Formation), support an early late Bajocian age[6,7].

In Cape Kystatym, the occurrence of the ammonite *Boreocephalites* cf. *laptinskaje* (Voronets) is reported 13 m above the glendonite-bearing layer[8]. In a recent revision of the evolution of the ammonite genera *Cranocephalites* of East Greenland[9], the specie *Morrisiceras laptinskaje Voronets* has been considered as corresponding to *Cranocephalites borealis* trans. β, which is the index species of the second horizon of the *Borealis* ammonite zone.

In Chekurovka, the ammonites *Arctocephalites arcticus* and *Oxycerites*[3] have been recognized ~60 m above the oldest glendonite-bearing beds belonging to the Kelimyar Formation. Age of the *Arcticus* ammonite zone can either be attributed to the uppermost Bajocian or to the lowermost Bathonian. An upper Bajocian age of glendonites is however suggested by comparison with other glendonite-bearing layers of the region (cf. Cape Kystatym).

3. Lower-middle Bathonian: Chucha, Chekurovka

In the Chekurovka section, the ammonite *Arcticoceras harlandi* (found ~75 m above the base of the Chekurovka Formation, respectively) typify the *Ischmae* ammonite zone. In addition, the ammonite *A.* cf. *ischmae* has been found at the top of the Chekurovka Fm in a nearby section (Chekurovka-North), indicating that most of the formation is ascribed to the *Ischmae* zone. A lower Bathonian age for at least part of the *Ischmae* zone has been evidenced in the Russian Platform (Saratov region), by the joint presence of the ammonites *Oraniceras* and *Arcticoceras*[10].

In the Chucha section, the occurrence of the ammonite *Cadoceras (Catacadoceras) barnstoni (Meek)* 4 m below the top of the Chekurovka Formation indicate a middle to upper Bathonian age. In the Chekurovka section, the record of the ammonite *Arcticoceras*

cranocephaloide 5 m below the top of the Chekurovka Formation indicates the middle Bathonian.

4. Upper Ryazanian: Chucha

In the Chucha section, the thick sandstone-dominated Ryazanian succession of the Khairgass Formation (~400 m) has delivered numerous bivalves *Buchia*[11]. All glendonite-bearing units belong to the *Bojarkia mesezhnikowi* zone, as they yield ammonites of the genus *Bojarkia*. This zone corresponds to the middle part of the *Subthurmannia boissieri* zone of the Tethyan zonal succession[12,13].

References

1 Suan, G. *et al.* Polar record of Early Jurassic massive carbon injection. *Earth and Planetary Science Letters* **312**, 102-113, doi:http://dx.doi.org/10.1016/j.epsl.2011.09.050 (2011).

2 Koshelkina, Z. V. Stratrigraphy and bivalves of the Jurassic deposits of Vilyui Syncline and Priverchoyanye depression. *Transactions of the North-East complex scientific ninstitute (SKVNII)* **5**, 219 (1963).

3 Meledina, S. V. *et al.* Chekurovka Formation (Bathonian-Callovian) in the Stratotype. *High-Resolution Jurassic-Cretaceous Stratigraphy and Paleontology of Siberia*, 5-36 (1991).

4 Nikitenko, B. L. *et al.* Jurassic and Cretaceous stratigraphy of the Anabar area (Arctic Siberia, Laptev Sea coast) and the Boreal zonal standard. *Russian Geology and Geophysics* **54**, 808-837, doi:http://dx.doi.org/10.1016/j.rgg.2013.07.005 (2013).

5 Callomon, J. H. The evolution of the Jurassic ammonite family Cardioceratidae. *Special papers in Palaeontology*, 49-90 (1985).

6 Engkilde, M. & Surlyk, F. Shallow marine syn-rift sedimentation: Middle Jurassic Pelion Formation, Jameson Land, East Greenland. *The Jurassic of Denmark and Greenland. Geological Survey of Denmark and Greenland Bulletin* **1**, 813-863 (2003).

7 McArthur, J. M., Howarth, R. J. & Bailey, T. R. Strontium isotope stratigraphy: LOWESS version 3: best fit to the marine Sr-isotope curve for 0–509 Ma and accompanying look-up table for deriving numerical age. *The Journal of Geology* **109**, 155-170 (2001).

8 Meledina, S. V. & Kirina, T. I. On stratigraphy of the Middle Jurassic deposits of the Lena river lower flows (Zhigansk area). *Trans. Inst. Geol: Geophys. Sib. Branch Ac. Sci. USSR.* **136**, 105-109 (1974).

9 Callomon, J. H., Alsen, P. & Surlyk, F. The ammonites of the Middle Jurassic Cranocephalites beds of East Greenland. *Geological Survey of Denmark & Greenland Bulletin* (2015).

10 Mitta, V. *et al.* Biostratigraphy and sedimentary settings of the Upper Bajocian-Lower Bathonian in the vicinity of Saratov (Central Russia). *Neues Jahrbuch für Geologie und Paläontologie-Abhandlungen* **271**, 95-121 (2014).

11 Rogov, M. A., Zakharov, V. A. & Ershova, V. B. Detailed stratigraphy of the Jurassic-Cretaceous boundary beds of the Lena River lower reached based on ammonites and Buchiids. *Stratigraphy and Geological Correlation* **19**, 641-662, doi:10.1134/S0869593811060050 (2011).

12 Baraboshkin, E. J. Boreal Tethyan correlation of Lower Cretaceous ammonites scales. *Moscow University Bulletin* **59**, 9-20 (2004).

13 Reboulet, S. *et al.* Report on the 5th International Meeting of the IUGS Lower Cretaceous Ammonite Working Group, the Kilian Group (Ankara, Turkey, 31st August 2013). *Cretaceous Research* **50**, 126-137 (2014).

Supplemental Information 4: Correlation of Boreal ammonite zones to the Geologic Time Scale (GTS)

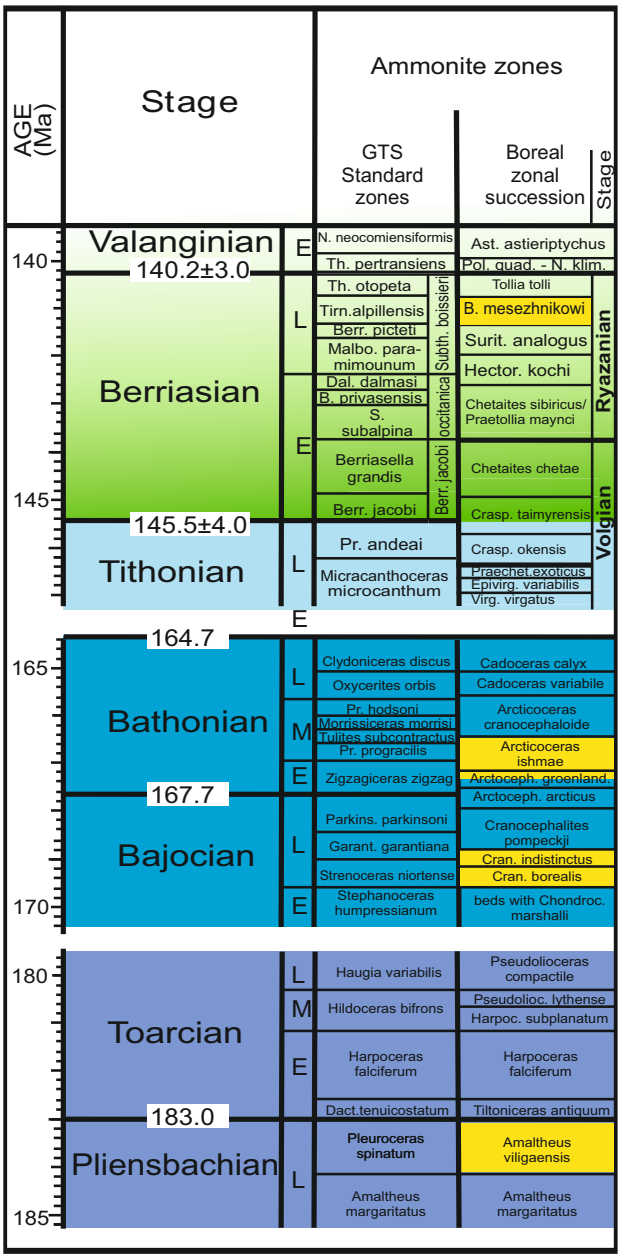

Supplemental Information 5: Methods

A total of 33 glendonite samples have been collected: 11 in Anabar Bay, 11 in Cape Kystatym, 3 in Cape Khorongkho, 5 in Chekurovka, and 3 in Chucha. All samples (glendonites, nodules and enclosing sediment) have been subjected to petrological, and carbon and oxygen isotope measurements. Rock-Eval analyses were performed on a representative set of 29 samples (glendonites and sediment), and compound-specific isotope analyses (CSIA) on 5 selected glendonite samples (see Supplementary Information for details on methods). Thin sections of 20µm have been made for all samples and petrographic microscopy analyses have been performed on a Leica DM600B equipped by a lamp CTR 6500 and a camera DFC350FX (from Leica, Wetzlar, Germany) and fitted with polarised and UV light.

Bulk-rock glendonites, carbonate nodules and host sediment isotope measurements have been performed on powder samples collected using a micro-drill on clean surfaces of rock slabs. The isotope measurements were carried out 1) in Utrecht University using an ISOCARB common acid bath carbonate preparation device linked on-line to a VG SIRA24 mass spectrometer; and 2) in Frankfurt University, using a Gas Bench II (Thermoquest) directly coupled to the continuous flow inlet system of the Finnigan MAT 253 mass spectrometer (Thermo Fisher Scientific, Waltham, MA, USA). Ratios of carbon and oxygen isotopes are reported in the delta (δ) notation as per mil (‰) deviation relative to the Vienna–Pee Dee belemnite standard (VPDB). Analytical precision was determined by replicate analyses and by comparison to international (IAEA-CO1 and NBS19 in Utrecht University; NBS18 and NBS19 in Frankfurt University) and in-house (NAXOS in Utrecht University; Carrara Marble in Frankfurt University) carbonate standards, showing standard deviations of <0.06‰ and <0.1‰ for $\delta^{13}C$ and $\delta^{18}O$, respectively.

Total organic carbon (TOC), T_{max}, and hydrogen and oxygen indices (HI and OI) were measured with a Rock-Eval 6 pyrolysis device with an instrumental precision of <2%. The T_{max} values (°C) indicate thermal maturity of the organic matter and allow the assessment of the diagenetic overprint (Espitalié et al., 1985). The peaks S2, S3 and S4 are used to calculate the amount of total organic carbon (TOC) and the amount of mineral carbon (MINC). The peaks S2 and S3 correspond to the pyrolysis phase (e.g. to the amount of kerogen and CO_2 released during cracking of organic-matter between 600 and 800 °C), and the peak S4 to the oxidation phase (residual TOC). In addition, the hydrogen index (HI =S2/TOC) and oxygen index (OI = S3/TOC) are calculated. The HI and OI indices are proportional to the H/C and O/C ratios of the organic matter, respectively, and are used for organic matter classification in Van-Krevelen-type diagrams (Espitalié et al., 1985, 1986). The analyses were calibrated by analysing the standard reference material IFP-160000 (Institut Français du Pétrole).

Compound Specific Isotope Analysis of the gas inclusions were measured using a custom build rock crusher interfaced with a GC-IRMS system. Around 1 gram of rock sample is introduced in the crusher, which after closing was flushed with Helium to remove air. During crushing a force of 30 MPa was applied to a plunger and the released gases were transported out of the crusher using a continuous Helium flow and subsequently trapped on a PLOT column dipped in liquid Nitrogen. At the start of the analysis the trap was heated and the components were injected into a HP 7890 GC. The components were separated on a PoraPLOT Q-HT column. The effluent of the GC was converted to CO_2 in a combustion furnace and injected in a MAT 253 mass spectrometer. The results of the IRMS were calibrated using reference CO_2, which was introduced in pulses during the analysis. An accuracy of at least +/- 0.5‰ was obtained.

Supplemental Information 6: Pseudo Van Krevelen diagram (Espitalier et al., 1985).

Tmax values (x axis, in °C, corresponding to the cracking temperature of the sedimentary organic matter and representating its degree of maturity) are plotted again the HI index (y axis, in mg HC/g TOC, indicative of the type of organic matter). For reliability sake, only data showing TOC ≥ 0.2 % (e.g. in the detection limit) are shown.

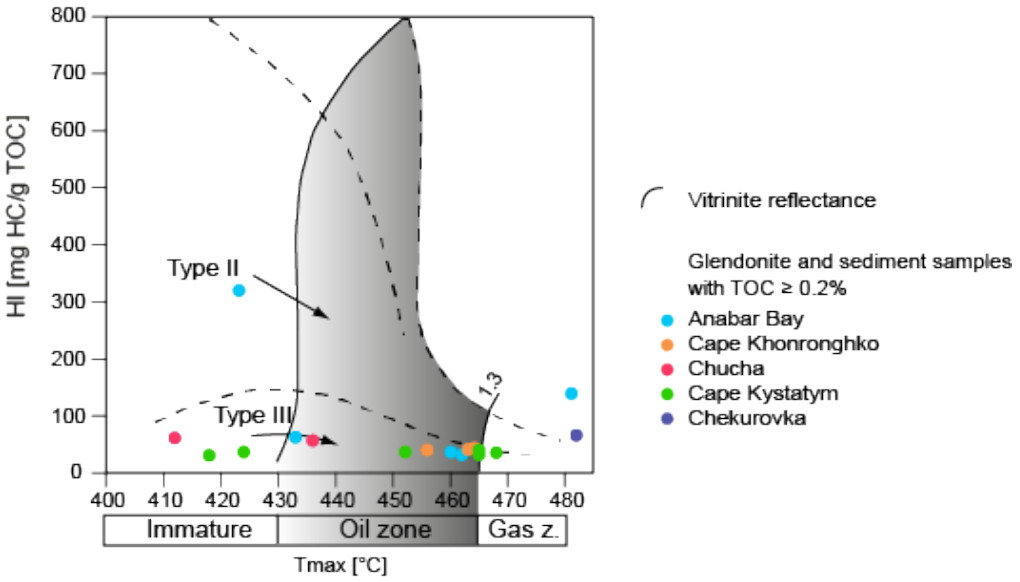

Supplemental Information 7: Details on CSIA performed on glendonites gas inclusions.

The diagrams show the molecular composition (in % of hydrocarbons) and carbon stable isotope values (in ‰ V-PDB) of hydrocarbon gas species trapped in bulk-glendonites.

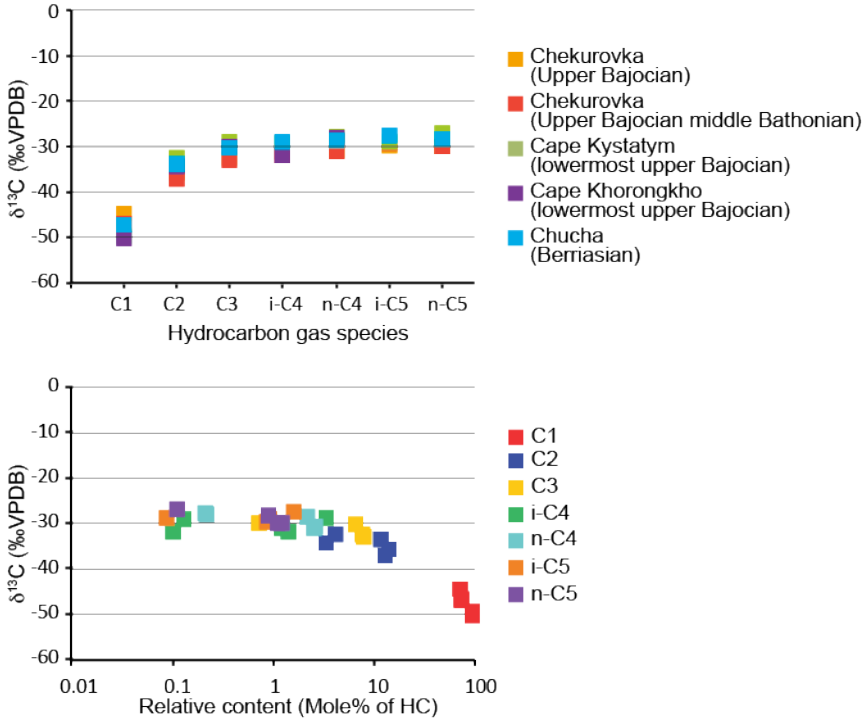

Raw carbon and oxygen stable isotope data of bulk-glendonites, nodules, and diagenetic carbonates of enclosing sediments

SECTION	TYPE OF SAMPLE	AGE	AMMONITE ZONE (when determined)	SAMPLE NUMBER	δ13C (‰ VPDB)	δ18O (‰ VPDB)	LAB OF ANALYSIS
Annabar Bay	Glendonite	Upper Pliensbachian	Amaltheus stokesi-A. viligaensis	B1G	-15.1	-5.2	Utrecht
Annabar Bay	Glendonite	Upper Pliensbachian	Amaltheus stokesi-A. viligaensis	B1G	-15.6	-7.2	Utrecht
Annabar Bay	Glendonite	Upper Pliensbachian	Amaltheus stokesi-A. viligaensis	B2G	-20.4	-2.0	Utrecht
Annabar Bay	Glendonite	Upper Pliensbachian	Amaltheus stokesi-A. viligaensis	B2G	-19.0	-3.3	Utrecht
Annabar Bay	Glendonite	Upper Pliensbachian	Amaltheus stokesi-A. viligaensis	B3G	-12.6	-9.9	Utrecht
Annabar Bay	Glendonite	Upper Pliensbachian	Amaltheus stokesi-A. viligaensis	B3G	-19.1	-7.1	Utrecht
Annabar Bay	Glendonite	Upper Pliensbachian	Amaltheus stokesi-A. viligaensis	B4G	-16.9	-8.1	Utrecht
Annabar Bay	Glendonite	Upper Pliensbachian	Amaltheus stokesi-A. viligaensis	B4G	-16.6	-7.2	Utrecht
Annabar Bay	Glendonite	Upper Pliensbachian		W13G	-23.3	-7.0	Utrecht
Annabar Bay	Glendonite	Upper Pliensbachian		W13G	-21.2	-9.4	Utrecht
Annabar Bay	Glendonite	Upper Pliensbachian		W14G	-37.31	-2.64	Frankfurt
Annabar Bay	Glendonite	Upper Pliensbachian		W15G	-30.25	-7.18	Frankfurt
Annabar Bay	Glendonite	Upper Pliensbachian		W15Gtop	-30.6	-7.5	Utrecht
Annabar Bay	Glendonite	Upper Pliensbachian		W16G	-31.2	-7.1	Utrecht
Annabar Bay	Glendonite	Upper Pliensbachian		W16G	-32.8	-5.3	Utrecht
Annabar Bay	Glendonite	Upper Pliensbachian		W17 G	-21.71	-5.87	Frankfurt
Annabar Bay	Glendonite	Upper Pliensbachian		W17G	-21.3	-4.9	Utrecht
Annabar Bay	Glendonite	Upper Pliensbachian		W17G	-22.0	-3.2	Utrecht
Annabar Bay	Glendonite	Upper Pliensbachian		W18G	-19.53	-7.17	Frankfurt
Annabar Bay	Glendonite	Upper Pliensbachian		W18Gbase	-21.0	-5.6	Utrecht
Annabar Bay	Glendonite	Upper Pliensbachian		W18Gtop	-17.4	-9.1	Utrecht
Annabar Bay	Glendonite	Upper Pliensbachian		W19G	-17.80	-7.08	Frankfurt
Annabar Bay	Glendonite	Upper Pliensbachian		W19G	-17.6	-8.1	Utrecht
Annabar Bay	Sediment	Upper Pliensbachian	Amaltheus stokesi-A. viligaensis	B2S	-9.69	-8.04	Frankfurt
Annabar Bay	Sediment	Upper Pliensbachian	Amaltheus stokesi-A. viligaensis	B2S	-18.1	-2.6	Utrecht
Annabar Bay	Sediment	Upper Pliensbachian	Amaltheus stokesi-A. viligaensis	B3S	-4.17	-10.17	Frankfurt
Annabar Bay	Sediment	Upper Pliensbachian	Amaltheus stokesi-A. viligaensis	B3S	-4.5	-10.8	Utrecht
Annabar Bay	Sediment	Upper Pliensbachian	Amaltheus stokesi-A. viligaensis	B4S	-3.39	-9.40	Frankfurt
Annabar Bay	Sediment	Upper Pliensbachian	Amaltheus stokesi-A. viligaensis	B4S	-3.3	-10.0	Utrecht
Annabar Bay	Sediment	Upper Pliensbachian		W13S	-10.2	-18.9	Utrecht
Annabar Bay	Sediment	Upper Pliensbachian		W16S	-8.4	-18.6	Utrecht
Annabar Bay	Sediment	Upper Pliensbachian		W17S	-5.06	-11.37	Frankfurt
Annabar Bay	Sediment	Upper Pliensbachian		W17S	-3.7	-10.8	Utrecht
Annabar Bay	Sediment	Upper Pliensbachian		W17Smicrite	-3.7	-11.1	Utrecht
Chekurovka	Glendonite	Upper Bajocian	not younger than Arctocephalites arcticus	W3G	-16.0	-7.8	Utrecht
Chekurovka	Glendonite	Upper Bajocian	not younger than Arctocephalites arcticus	W3G	-5.7	-11.3	Utrecht

SECTION	TYPE OF SAMPLE	AGE	AMMONITE ZONE (when determined)	SAMPLE NUMBER	δ13C (‰ VPDB)	δ18O (‰ VPDB)	LAB OF ANALYSIS
Chekurovka	Glendonite	Upper Bajocian	not younger than Arctocephalites arcticus	W10G	-18.57	-5.14	Frankfurt
Chekurovka	Glendonite	Upper Bajocian	not younger than Arctocephalites arcticus	W10G	-13.1	-10.3	Utrecht
Chekurovka	Glendonite	Upper Bajocian	not younger than Arctocephalites arcticus	W10G	-19.6	-4.9	Utrecht
Chekurovka	Glendonite	uppermost lower-middle Batho.	Arcticoceras harlandi-A. cranocephaloide interval	W11G	-14.5	-10.7	Utrecht
Chekurovka	Glendonite	uppermost lower-middle Batho.	Arcticoceras harlandi-A. cranocephaloide interval	W11G	-17.2	-8.3	Utrecht
Chekurovka	Glendonite	uppermost lower-middle Batho.	Arcticoceras harlandi-A. cranocephaloide interval	W1G	-30.6	-5.5	Utrecht
Chekurovka	Glendonite	uppermost lower-middle Batho.	Arcticoceras harlandi-A. cranocephaloide interval	W1G	-28.4	-4.9	Utrecht
Chekurovka	Glendonite	Upper Bajocian-Middle Bathonian	*block not in place*	W12G	-12.8	-8.2	Utrecht
Chekurovka	Glendonite	Upper Bajocian-Middle Bathonian	*block not in place*	W12G	-16.4	-5.8	Utrecht
Chekurovka	Nodule	uppermost lower-middle Batho.	Arcticoceras harlandi-A. cranocephaloide interval	W1N	-30.4	-4.0	Utrecht
Chekurovka	Sediment	Upper Bajocian	not younger than Arctocephalites arcticus	W10S	-2.04	-8.24	Frankfurt
Chekurovka	Sediment	Upper Bajocian	not younger than Arctocephalites arcticus	W10S	-3.0	-9.1	Utrecht
Chekurovka	Sediment	Upper Bajocian	not younger than Arctocephalites arcticus	W2 S	19.17	-6.93	Frankfurt
Chekurovka	Sediment	Upper Bajocian	not younger than Arctocephalites arcticus	W2S	21.3	-6.0	Utrecht
Chekurovka	Sediment	uppermost lower-middle Batho.	Arcticoceras harlandi-A. cranocephaloide interval	W1S	-29.45	-3.74	Frankfurt
Chucha	Glendonite	Lower Bathonian?	Arcticoceras ishmae?	W6G	-21.6	-6.7	Utrecht
Chucha	Glendonite	Lower Bathonian?	Arcticoceras ishmae?	W8G	-21.5	-6.0	Utrecht
Chucha	Glendonite	Berriasian	Mesezhnikovi or Analogus zone	W35G	-22.8	-8.8	Utrecht
Chucha	Glendonite	Berriasian	Mesezhnikovi or Analogus zone	W35G	-19.7	-7.9	Utrecht
Chucha	Nodule	Berriasian	Mesezhnikovi or Analogus zone	W35N	-24.0	-3.4	Utrecht
Chucha	Sediment	Lower Bathonian?	Arcticoceras ishmae?	W6S	-2.87	-17.77	Frankfurt
Chucha	Sediment	Lower Bathonian?	Arcticoceras ishmae?	W6S	-5.0	-18.6	Utrecht
Chucha	Sediment	Lower Bathonian?	Arcticoceras ishmae?	W7S	-2.69	-17.82	Frankfurt
Cape Kystatym	Glendonite	lowermost upper Bajocian	lower part of Boreiocephalites pseudoborealis	W22bG	-18.3	-2.3	Utrecht
Cape Kystatym	Glendonite	lowermost upper Bajocian	lower part of Boreiocephalites pseudoborealis	W23a-1G	-22.6	-1.6	Utrecht
Cape Kystatym	Glendonite	lowermost upper Bajocian	lower part of Boreiocephalites pseudoborealis	W23a-1G	-20.4	-1.9	Utrecht
Cape Kystatym	Glendonite	lowermost upper Bajocian	lower part of Boreiocephalites pseudoborealis	W23a-1G	-23.9	-1.8	Utrecht
Cape Kystatym	Glendonite	lowermost upper Bajocian	lower part of Boreiocephalites pseudoborealis	W23a-2G	-23.8	-1.9	Utrecht
Cape Kystatym	Glendonite	lowermost upper Bajocian	lower part of Boreiocephalites pseudoborealis	W23a-2G	-24.9	-0.8	Utrecht
Cape Kystatym	Glendonite	lowermost upper Bajocian	lower part of Boreiocephalites pseudoborealis	W23b-1G	-15.9	-4.2	Utrecht
Cape Kystatym	Glendonite	lowermost upper Bajocian	lower part of Boreiocephalites pseudoborealis	W23bG	-16.4	-3.9	Utrecht
Cape Kystatym	Glendonite	lowermost upper Bajocian	lower part of Boreiocephalites pseudoborealis	W24G	-7.0	-10.8	Utrecht
Cape Kystatym	Glendonite	lowermost upper Bajocian	lower part of Boreiocephalites pseudoborealis	W24G	-0.4	-14.7	Utrecht
Cape Kystatym	Glendonite	lowermost upper Bajocian	lower part of Boreiocephalites pseudoborealis	W25G	-22.3	-2.4	Utrecht
Cape Kystatym	Glendonite	lowermost upper Bajocian	lower part of Boreiocephalites pseudoborealis	W25G	-9.6	-10.1	Utrecht
Cape Kystatym	Glendonite	lowermost upper Bajocian	lower part of Boreiocephalites pseudoborealis	W25Gd	-18.4	-4.5	Utrecht

SECTION	TYPE OF SAMPLE	AGE	AMMONITE ZONE (when determined)	SAMPLE NUMBER	δ13C (‰ VPDB)	δ18O (‰ VPDB)	LAB OF ANALYSIS
Cape Kystatym	Glendonite	lowermost upper Bajocian	lower part of Boreiocephalites pseudoborealis	W27G	-23.6	-1.6	Utrecht
Cape Kystatym	Glendonite	lowermost upper Bajocian	lower part of Boreiocephalites pseudoborealis	W27G	-23.9	-1.5	Utrecht
Cape Kystatym	Glendonite	lowermost upper Bajocian?	*block not in place*	W20G	-12.9	-8.2	Utrecht
Cape Kystatym	Glendonite	lowermost upper Bajocian?	*block not in place*	W30b	-44.2	-3.9	Utrecht
Cape Kystatym	Glendonite	lowermost upper Bajocian?	*block not in place*	W30b	-44.5	-1.3	Utrecht
Cape Kystatym	Glendonite	lowermost upper Bajocian?	*block not in place*	W31G	-27.7	-5.8	Utrecht
Cape Kystatym	Glendonite	lowermost upper Bajocian?	*block not in place*	W31G	-39.6	-2.5	Utrecht
Cape Kystatym	Nodule	lowermost upper Bajocian	lower part of Boreiocephalites pseudoborealis	W23b-2N	-17.65	-2.73	Frankfurt
Cape Kystatym	Nodule	lowermost upper Bajocian	lower part of Boreiocephalites pseudoborealis	W23b-1N	-16.4	-3.3	Utrecht
Cape Kystatym	Sediment	lowermost upper Bajocian	lower part of Boreiocephalites pseudoborealis	W24S	13.77	-18.46	Frankfurt
Cape Kystatym	Sediment	lowermost upper Bajocian	lower part of Boreiocephalites pseudoborealis	W24S	9.7	-19.4	Utrecht
Cape Kystatym	Sediment	lowermost upper Bajocian	lower part of Boreiocephalites pseudoborealis	W24Smicrite	11.0	-16.7	Utrecht
Cape Kystatym	Sediment	lowermost upper Bajocian	lower part of Boreiocephalites pseudoborealis	W25S	11.89	-15.52	Frankfurt
Cape Kystatym	Sediment	lowermost upper Bajocian	lower part of Boreiocephalites pseudoborealis	W25S	11.6	-14.6	Utrecht
Cape Kystatym	Sediment	lowermost upper Bajocian	lower part of Boreiocephalites pseudoborealis	W27S	-18.1	-3.3	Utrecht
Cape Kystatym	Sediment	lowermost upper Bajocian	lower part of Boreiocephalites pseudoborealis	W29S	13.75	-18.98	Frankfurt
Cape Kystatym	Sediment	lowermost upper Bajocian	lower part of Boreiocephalites pseudoborealis	W29S	15.4	-17.9	Utrecht
Cape Kystatym	Sediment	lowermost upper Bajocian	lower part of Boreiocephalites pseudoborealis	W30S	-12.3	-13.5	Utrecht
Cape Kystatym	Sediment	lowermost upper Bajocian	lower part of Boreiocephalites pseudoborealis	W22bS	14.98	-16.57	Frankfurt
Cape Kystatym	Sediment	lowermost upper Bajocian	lower part of Boreiocephalites pseudoborealis	W22bS	15.4	-16.1	Utrecht
Cape Kystatym	Sediment	lowermost upper Bajocian	lower part of Boreiocephalites pseudoborealis	W22bS	15.0	-16.2	Utrecht
Cape Kystatym	Sediment	lowermost upper Bajocian?	*block not in place*	W20S	12.52	-14.83	Frankfurt
Cape Kystatym	Sediment	lowermost upper Bajocian?	*block not in place*	W20S	11.4	-14.8	Utrecht
Cape Khorongkho	Glendonite	lowermost upper Bajocian	Boreiocephalites pseudoborealis?	W32G	-18.6	-4.6	Utrecht
Cape Khorongkho	Glendonite	lowermost upper Bajocian	Boreiocephalites pseudoborealis?	W32G	0.0	-9.8	Utrecht
Cape Khorongkho	Glendonite	lowermost upper Bajocian	Boreiocephalites pseudoborealis?	W32G	-9.9	-9.4	Utrecht
Cape Khorongkho	Glendonite	lowermost upper Bajocian	Boreiocephalites pseudoborealis?	W32G	-5.8	-8.0	Utrecht
Cape Khorongkho	Glendonite	lowermost upper Bajocian	Boreiocephalites pseudoborealis?	W33G	-22.6	-2.9	Utrecht
Cape Khorongkho	Glendonite	lowermost upper Bajocian	Boreiocephalites pseudoborealis?	W33G	-16.7	-5.9	Utrecht
Cape Khorongkho	Glendonite	lowermost upper Bajocian	Boreiocephalites pseudoborealis?	W34G	-12.1	-6.4	Utrecht
Cape Khorongkho	Glendonite	lowermost upper Bajocian	Boreiocephalites pseudoborealis?	W34G	-13.1	-5.7	Utrecht
Cape Khorongkho	Sediment	lowermost upper Bajocian	Boreiocephalites pseudoborealis?	W32S	12.24	-16.13	Frankfurt
Cape Khorongkho	Sediment	lowermost upper Bajocian	Boreiocephalites pseudoborealis?	W32S	12.2	-16.1	Utrecht
Cape Khorongkho	Sediment	lowermost upper Bajocian	Boreiocephalites pseudoborealis?	W32S	10.3	-20.6	Utrecht
Cape Khorongkho	Sediment	lowermost upper Bajocian	Boreiocephalites pseudoborealis?	W33S	10.94	-17.94	Frankfurt
Cape Khorongkho	Sediment	lowermost upper Bajocian	Boreiocephalites pseudoborealis?	W33S	11.6	-18.1	Utrecht
Cape Khorongkho	Sediment	lowermost upper Bajocian	Boreiocephalites pseudoborealis?	W34S	12.39	-15.83	Frankfurt
Cape Khorongkho	Sediment	lowermost upper Bajocian	Boreiocephalites pseudoborealis?	W34S	11.6	-16.3	Utrecht

Raw Rock-Eval data

Samples	Type	Section	TOC [%]	HI [mg HC/g TOC]	OI [mg CO2/g TOC]	Tmax [°C]	S1 [mg HC/g]	S2a [mg HC/g]	S2b [mg HC/g]	S3
B1	Glendonite	Anabar Bay	0.37	63	211	433	0.01	0.23	0.00	0.78
B2	Sediment	Anabar Bay	0.55	37	172	460	0.02	0.20	0.00	0.94
B4	Sediment	Anabar Bay	0.02	320	2532	423	0.01	0.06	0.00	0.46
W17	Glendonite	Anabar Bay	0.35	33	459	462	0.01	0.12	0.00	1.63
W18	Glendonite	Anabar Bay	0.08	140	830	481	0.01	0.12	0.00	0.69
W2	Sediment	Chekurovka	0.78	67	112	482	0.09	0.53	0.00	0.88
W20	Sediment	Cape Kystatym	0.25	31	368	418	0.01	0.08	0.00	0.94
W23B1	Glendonite	Cape Kystatym	0.52	37	355	452	0.01	0.20	0.00	1.86
W23B	Nodule	Cape Kystatym	0.41	36	376	468	0.01	0.15	0.00	1.54
W24	Sediment	Cape Kystatym	0.33	41	190	465	0.01	0.14	0.00	0.63
W25	Sediment	Cape Kystatym	0.35	37	221	424	0.01	0.13	0.00	0.77
W29	Sediment	Cape Kystatym	0.61	32	245	465	0.01	0.20	0.00	1.49
W32	Sediment	Cape Khorongkho	0.39	41	271	456	0.01	0.16	0.00	1.05
W33	Sediment	Cape Khorongkho	0.46	44	163	464	0.01	0.21	0.00	0.75
W34	Sediment	Cape Khorongkho	0.56	42	206	463	0.01	0.23	0.00	1.15
W35	Glendonite	Chucha	0.30	62	239	412	0.03	0.19	0.00	0.72
W8	Sediment	Chucha	0.24	57	66	436	0.03	0.14	0.00	0.16

Raw CSIA data performed on bulk-glendonites gas inclusions

AGE	SECTION	SAMPLE	Gas composition [mole%] (Total hydrocarbons = 100%)						
			C1	C2	C3	i-C_4	n-C_4	i-C_5	n-C_5
upper Bajocian	Chekurovka	W10	72.4	14.1	7.7	1.2	2.6	0.86	1.1
up. Baj.-mid. Bathonian	Chekurovka	W12	73.4	12.8	7.8	1.4	2.5	0.93	1.2
upper Bajocian	Cape Kystatym	W23a2	94.3	4.2	0.89	0.13	0.21	0.087	0.11
upper Bajocian	Cape Khorongkho	W33	95.3	3.3	0.72	0.1	0.22	0.074	0.1
Berriasian	Chucha	W35	73.6	11.9	6.5	3.3	2.2	1.6	0.9

AGE	SECTION	SAMPLE	Carbon isotope ratios (δ13C ‰ VPDB)						
			C1	C2	C3	i-C_4	n-C_4	i-C_5	n-C_5
upper Bajocian	Chekurovka	W10	-44.7	-35.7	-32.5	-31.2	-30.8	-29.7	-30.1
up. Baj.-mid. Bathonian	Chekurovka	W12	-46.9	-37.2	-33.0	-32.0	-31.2	-29.3	-30.0
upper Bajocian	Cape Kystatym	W23a2	-49.6	-32.5	-28.9	-29.3	-27.7	-29	-27
upper Bajocian	Cape Khorongkho	W33	-50.3	-34.4	-30.0	-32	-28		
Berriasian	Chucha	W35	-47.2	-33.7	-30.3	-29.0	-28.7	-27.6	-28.4